small methods
www.small-methods.com

Stable Interface between Lithium and Electrolyte Facilitated by a Nanocomposite Protective Layer

Luyi Yang, Yongli Song, Hao Liu, Zijian Wang, Kai Yang, Qinghe Zhao, Yanhui Cui, Jiayun Wen, Wei Luo, and Feng Pan**

Recently, solid-state lithium batteries (SSLBs) have been considered an ideal solution for the practical application of lithium (Li) metal batteries owing to the excellent safety features of solid-state electrolytes (SSEs). Among various SSEs, Na superionic conductor (NASICON)-type $Li_{1+x}Al_xTi_{2-x}(PO_4)_3$ (LATP) holds great potential for its high ionic conductivity, low costs, and high stability. However, LATP tends to be reduced by metallic Li upon contact, posing a major challenge. Herein, a novel coating strategy is proposed to form a nanocomposite protecting layer on Li metal within 30 s. Such a protecting layer not only acts as an artificial solid-electrolyte interface to conduct Li ion transportation that remains stable after repeated cycling but also effectively precludes the interfacial reaction between Li and LATP by inhibiting the interfacial electron transfer. As a result, the Li/LATP/Li symmetric cells exhibit excellent cycling stability for over 300 h of continuous Li plating/stripping. The assembled full-cell using coated Li also shows high capacity retention after 500 cycles. Overall, this study demonstrates a facile and transferable method to reduce the reactivity of Li metal anode toward solid electrolytes with relatively high reduction potentials.

With the ever-increasing demand for energy storage system, next-generation battery systems with higher energy densities are desirable to replace traditional lithium-ion batteries (LIBs).[1] Due to its high theoretical capacity (3860 mAh g^{-1}) as well as low redox potential (−3.04 V vs standard hydrogen electrode), lithium (Li) metal is considered the ideal anode material for the next-generation battery.[2] However, the practical use of Li metal anode in organic liquid electrolyte is hindered by several issues such as low coulombic efficiency and unstable solid-electrolyte interface (SEI).[3] Moreover, safety issues related to the high flammability of organic liquid electrolyte and dendritic Li formation are also serious concerns when Li metal-based batteries are applied in electric vehicles.[4–6]

Recently, solid-state lithium batteries (SSLBs) have been extensively studied owing to the excellent safety features of solid-state electrolytes (SSEs). Moreover, it is widely believed that dendrite problem can be solved in SSLBs due to the enough mechanical strength of SSEs.[7–10] Thus, combining SSEs with Li metal anode is promising to deliver high safety and high energy density. Among various SSEs, Na superionic conductor (NASICON)-type $Li_{1+x}Al_xTi_{2-x}(PO_4)_3$ (LATP) with high room-temperature ionic conductivity, low costs and high stability in ambient environment are considered one of the most promising solid electrolytes.[11,12] These properties exhibit huge application potentials in next-generation Li metal batteries (e.g., Li–O_2 battery).[13,14] However, several disadvantages have limited the wide application of LATP such as the large grain boundary resistance as well as the Li loss during high-temperature sintering.[15,16] More importantly, due to the high reducibility of metallic Li, Li metal anode tends to irreversibly react with LATP directly.[17] As a result, severe side reactions between LATP and Li metal still remain a critical challenge where Ti^{4+} in LATP is prone to be reduced into Ti^{3+} by Li metal upon physical contact. The impurity phases and cracks resulted from the reduction reaction of LATP will lead to large interfacial resistance and eventually results in the failure of battery.[18–20] To improve the stability of NASICON-type SSEs against Li metal, intermediate layers including Ge,[21] crosslinked poly(ethylene glycol) methyl ether acrylate,[22] atomic-layer deposited Al_2O_3,[23] and boron nitride film[24] have been previously utilized at the interface between SSEs and Li metal foil. Alternatively, composite solid electrolytes such as poly(ethylene oxide), polyacrylonitrile, and poly(vinylidene fluoride-*co*-hexefluoropropylene) have also been reported by mixing LATP with solid polymer electrolytes.[25–30] Although both reported strategies could effectively mitigate the surface reduction reaction by avoiding direct contact between LATP and metallic Li, most techniques either require complex preparation process or compromise the energy density.

It has been widely reported that metal fluorides (e.g., LiF) play a crucial role in forming a stable SEI layer.[3] In this work,

Dr. L. Yang, Dr. Y. Song, H. Liu, Z. Wang, K. Yang, Dr. Q. Zhao, Dr. Y. Cui, Prof. F. Pan
School of Advanced Materials
Peking University Shenzhen Graduate School
Shenzhen 518055, P. R. China
E-mail: panfeng@pkusz.edu.cn
J. Wen, Prof. W. Luo
Institute of New Energy for Vehicles
School of Materials Science and Engineering
Tongji University
Shanghai 201804, P. R. China
E-mail: weiluo@tongji.edu.cn
The ORCID identification number(s) for the author(s) of this article can be found under https://doi.org/10.1002/smtd.201900751.

DOI: 10.1002/smtd.201900751

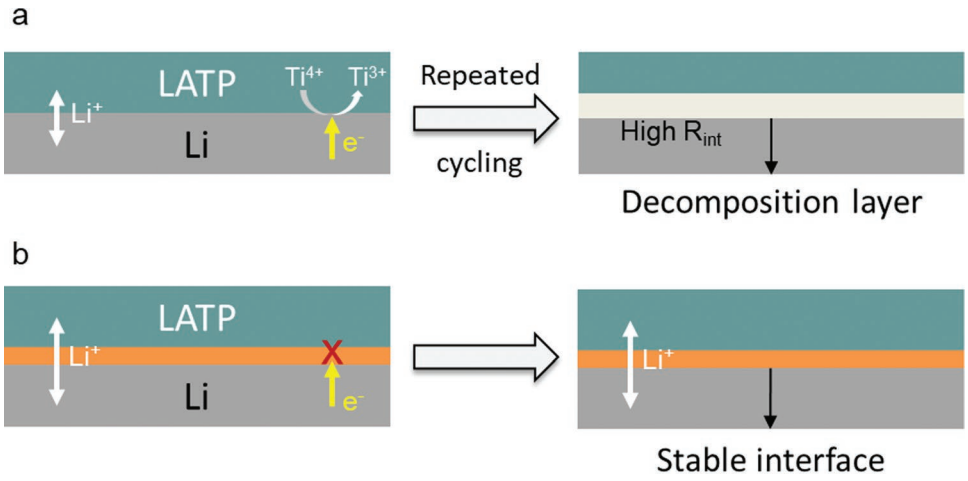

Figure 1. Schematic illustration of the LATP-Li interface with a) bare Li and b) coated Li: Ti^{4+} in LATP is continuously reduced by bare Li, forming a decomposition layer and leading to a high interfacial resistance; whereas the electron transfer is blocked by the coating layer, therefore a stable interface can be obtained.

a facile and rapid coating strategy is proposed to quickly form a nanocomposite protecting layer consisting of MgF_2, LiF, and B_2O_3 on Li metal. This layer serves as an artificial SEI which shields electron transfer and retards the reaction between Li and LATP. As demonstrated in **Figure 1**a, Li metal can reduce LATP and form a composition layer, which would further lead to an increasing interfacial impedance. In sharp contrast, by applying this coating layer at the Li/LATP interface, the electron transfer is inhibited (Figure 1b), hence the interfacial degradation is minimized, exhibiting excellent cycling stability for over 300 h of continuous Li plating/stripping. The $LiFePO_4$ (LFP)/LATP/Li battery also show high capacity retention after 500 cycles. The novel coating method presented in this work sheds lights to creating a more stable interface between Li metal and SSEs.

The coating process is illustrated in **Figure 2**a: first, a few drops of reaction solution containing $LiBF_4$ and $Mg(ClO_4)_2$ in dimethoxy ethane (DME) are casted on the Li metal foil; then the surface of Li foil turns dark immediately; after 30 s, the foil is washed by DME solvent and dried for use. The whole preparation takes less than 2 min, which is highly efficient for large-scale production. The cross-sectional scanning electron microscopy (SEM) image of the coated Li in Figure 2b shows that the thickness of the coating layer is ≈400 nm. However, by examining the coated Li using X-ray diffractometer (XRD), no extra peak other than metallic Li can be found (shown in Figure S1, Supporting Information). This may be due to that the coating layer is too thin to be detected by XRD. To determine the chemical compositions of the coating layer, a small amount of Li was employed to react with a large excess amount of reaction solution and the resulted solid product was collected for characterization. From the XRD pattern in Figure 2c, it can be seen that all metallic Li has fully reacted, forming LiF, MgF_2, and B_2O_3. This composition matches well with the X-ray photoelectron spectroscopy (XPS) data exhibited in Figure 2d,e (other elements are presented in Figure S2, Supporting Information), where Mg mainly exists as MgF_2 and B mainly exists as B_2O_3 with a small amount of BF_4^- residue. It is interesting that both $LiBF_4$ and $Mg(ClO_4)_2$ solutions are relatively stable with Li metal whereas the mixed solution reacts violently with Li within seconds. It is speculated that these two salts have synergic reactions with Li metal; however, the chemistry behind the reactions is still unclear.

The cycling stability of coated Li is first tested in Li-symmetric cells using ether-based liquid electrolyte consisting of 1.0 M lithium bis(fluorosulfonyl)imide (LiFSI) in DME. The voltage profiles of Li-symmetric cells using bare Li and coated Li are compared in Figure S3 in the Supporting Information. Under a current density of 1 mA cm^{-2}, the voltage polarization of the cell using bare Li increases gradually with time, suggesting a continuously increasing cell resistance. This can be attributed to the unstable SEI formed on the Li anode which results in accumulation of SEI as well as continuous consumption of electrolyte. The voltage spikes after 650 h of cycling, indicating a sudden deterioration of cell. Under the same testing condition, the cell with coated Li exhibits stable voltage profiles for 650 h of cycling despite that the initial polarization is higher than the cell with bare Li, which is due to the initial higher charge transfer resistance (R_{CT}) as evidenced in Figure S4 in the Supporting Information. In addition, as shown in Figure S5 in the Supporting Information, the coated Li maintained stable under a much higher areal capacity of 3 mAh cm^{-2} for over 100 h. Although the slightly impeded Li-ion transfer across the coating layer might be the origin of higher R_{CT} value, the significantly improved cycling stability indicates a well-preserved integrity of SEI in the presence of the coating layer. Moreover, from the XPS data (Figure 2f,g) of the coated Li after 100 cycles (washed by DME before XPS measurement), it can be concluded that the coating layer is able to endure repeated Li plating and stripping. In addition, the XPS data of C and F (Figure S6, Supporting Information) also show that the organic SEI component on Li surface barely changed after cycling, which further confirms the robust feature of the coating layer. By quantitatively analyzing the peak areas, it can be also found that the proportion of residue BF_4^- decreases from roughly 32% (31.6% of B and 32.1% of F) to ≈11% (10.8% of B and 11.7%

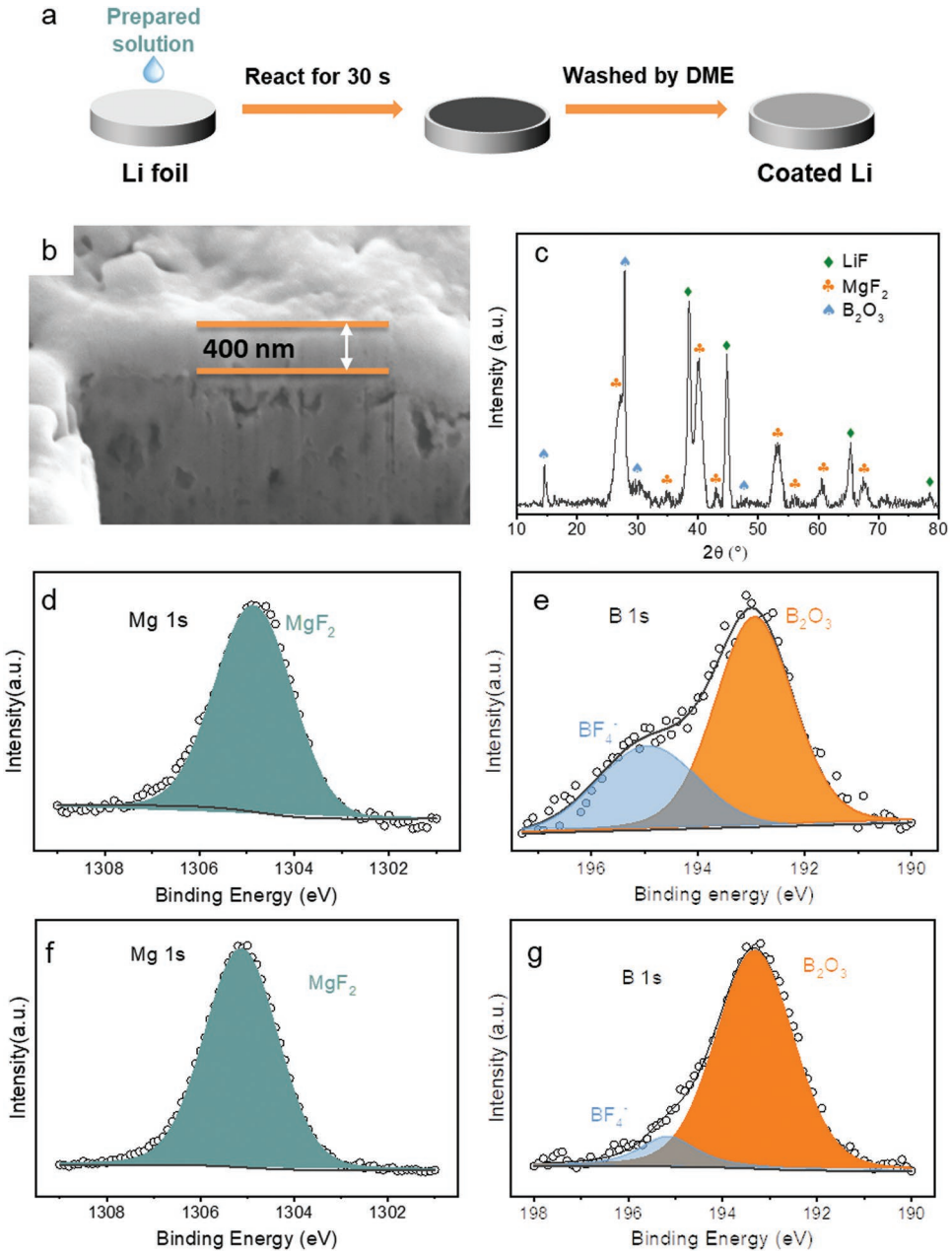

Figure 2. a) Schematic illustration of the coating process to prepare coated Li. b) Cross-sectional SEM image of coated Li after focus ion beam (FIB) cutting. c) XRD pattern of the solid product obtained from reacting a small amount of Li with a large excess amount of solution. XPS data of the coated Li d–e) before cycling and f–g) after 100 cycles in liquid electrolyte.

of F) after cycling, which can be due to that BF_4^- dissolves into the electrolyte during repeated reaction.

As shown in Figure S7 in the Supporting Information, the ionic conductivity of the prepared LATP pallet at room temperature is measured to be 2.35×10^{-4} S cm^{-1}, which is in good agreement with literature values (ranging from 8×10^{-5} to 6×10^{-4} S cm^{-1}).[31] To evaluate the chemical stability of LATP toward coated Li, Li symmetric cells are assembled where an LATP pellet is sandwiched between two Li anodes. It should be noted that due to the large impedances between solid-solid interfaces, a minimum amount (5 µL) of liquid electrolyte was added on each side of LATP pellet to wet the interface so that high-temperature sintering can be avoided. First, the electrochemical impedance spectra (EIS) of the cells are measured every 20 h after cell fabrication. From the Nyquist plot in **Figure 3**a, it can be seen that in the presence of bare Li, both the resistance of the bulk electrolyte R_E (presented by the starting point the semicircle in the Nyquist plot) and the interfacial impedance R_{Int} (presented by the semicircle in the Nyquist plot) increase drastically with time. This result suggests that the reaction between Li and LATP not only forms a layer of decomposition product with growing thickness

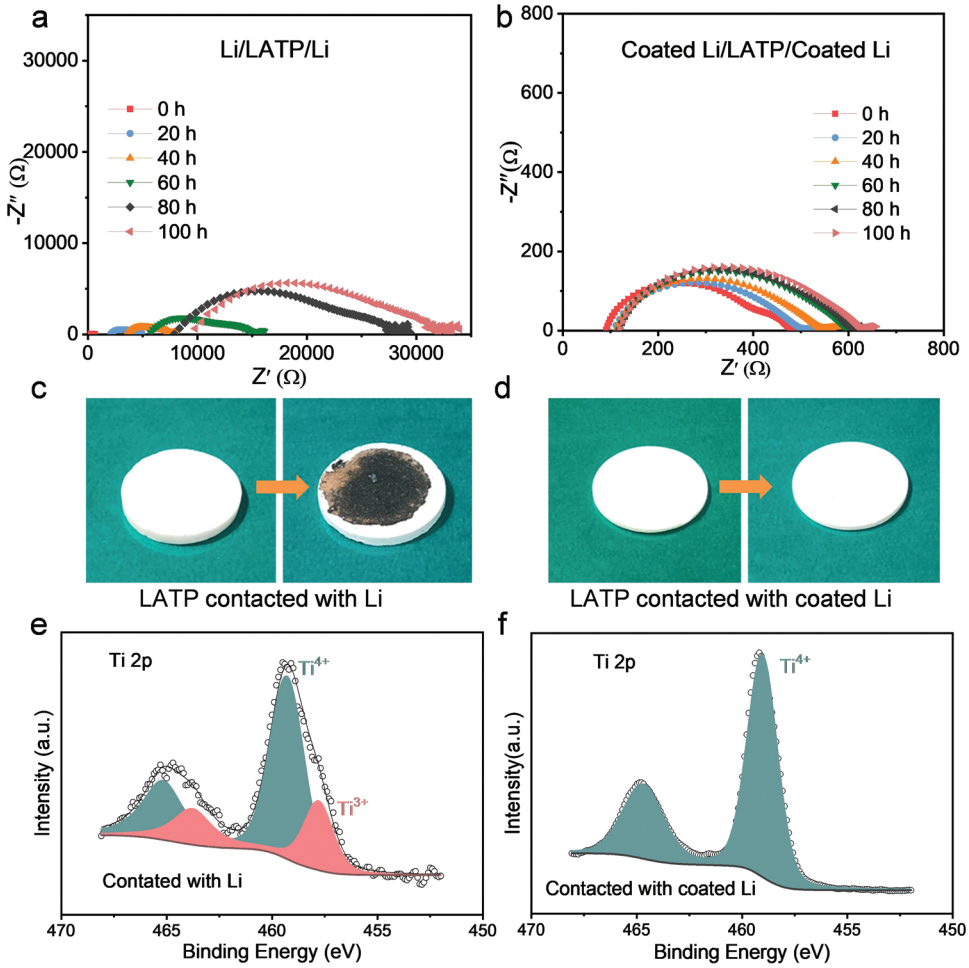

Figure 3. Electrochemical impedance sepctra of LATP-Li symmetric cells with a) bare Li and b) coated Li at different time. Photos of LATP pallet with the face in contact with c) bare Li and d) coated Li. XPS data of LATP pallet with the face in contact with e) bare Li and f) coated Li.

contributing to higher R_{Int} but also may causes microcracks in LATP resulting in higher R_E.[18] However, by replacing bare Li with the coated Li, the value of R_E and R_{Int} shown in Figure 3b only increased by 29 and 117 Ω, respectively. In addition, as shown in Figure 3c,d, it can be clearly observed that after 100 h, the surface of LATP contacted with Li turns black whereas the color of LATP contacted with coated Li remains unchanged. Moreover, the XPS results also confirm that Ti^{4+} at the interface is reduced to Ti^{3+} by the bare Li; whereas this phenomenon cannot be observed for LATP contacted with the coated Li. All evidences above strongly indicate suppressed reaction between LATP and coated Li, hence a more stable interface.

Galvanostatic cycling of Li symmetric cells is carried out to further test the interfacial stability between LATP and coated Li. The voltage profiles in **Figure 4**a clearly show that under a current density of 0.13 mA cm^{-2}, the voltage polarization of the Li/LATP/Li cell increases rapidly with cycles, which is in good accordance with the exacerbated interface. In sharp contrast, the voltage profiles of the cell using coated Li remain stable even after 300 h of cycling. The change impedance spectra with cycling (shown in Figure 4b,c) also indicate the huge difference between two cells. The interfacial stability is further demonstrated by testing the cell under a much higher current density (0.39 mA cm^{-2}) and areal capacity (0.39 mAh cm^{-2}), it is shown in Figure 4d that the voltage profiles remain stable after cycling for 75 h. It is also found that the compactness of coating layer also plays an important role in the interfacial stability between Li and LATP. As shown in Figure S8 in the Supporting Information, the color changes indicate that the increasing amount of solution added to react with Li promotes the thickness and compactness of the coating layer, hence the more stable Li/LATP interface.

For a better understanding of the protecting mechanism of the coating layer, its impact on electronic conductivity is evaluated via a potentiostatic method. By applying a constant external positive voltage (0.1 V) over a stainless steel (SS)/Li cell where two metals are directly contacted, a current contributed by electrons can be obtained. As shown in Figure S9 in the Supporting Information, electronic currents for SS/Li and SS/coated Li are the current 8×10^{-2} and 3×10^{-5} A respectively, indicating that the electronic conductivity of the cell is over 2000 times lower with the coating. Therefore, the key effect of the coating layer on stabilizing Li/LATP interface can be attributed to the inhibited electron transfer as illustrated in Figure 1.

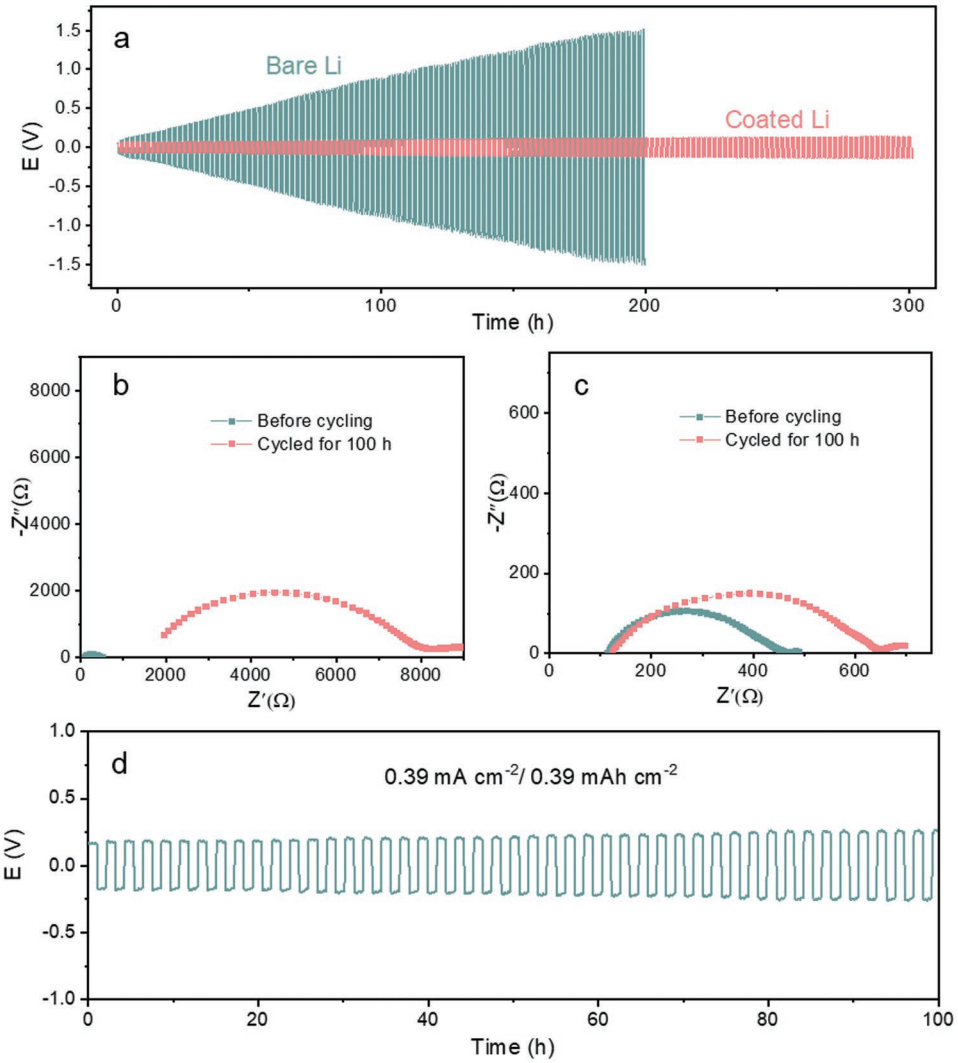

Figure 4. a) Voltage profiles of LATP-Li symmetric cells with bare Li and coated Li at a current density of 0.13 mA cm^{-2} and an areal capacity of 0.065 mAh g^{-1}; the areal capacity is electrochemical impedance spectra of the LATP-Li symmetric cells using b) bare Li and c) coated Li before cycling and after cycled for 100 h. d) Voltage profiles of Li symmetric cells with LATP using coated Li during long-term galvanostatic cycling at the current density of 0.39 mA cm^{-2} and areal capacity of 0.39 mAh cm^{-2}.

To evaluate the feasibility of this coating approach in a practical system, LFP full cells are further fabricated for long-term cycling at the rate of 1.5 C. As shown in **Figure 5**a, for the LFP/LATP/Li cell, the initial specific capacity is 150 mAh g^{-1}. Then the specific capacity of cell rapidly decreases as the cycle increases, the specific capacities of 50th cycle and 100th cycle are 69 and 11 mAh g^{-1} corresponding to a capacity retention of 45.5% and 7.4% respectively. From the previous results, it can be inferred that the failure of LFP/LATP/Li cell is attributed to the increased internal resistance caused by the reduction reaction between Li anode and LATP. By contrast, as shown in Figure 5b, despite the relatively low initial specific capacity of 130 mAh g^{-1}, the capacity of 17th cycle increases to 145 mAh g^{-1} after activation. More importantly, the specific capacities for 100th and 500th cycle are 136 and 127 mAh g^{-1} respectively, indicating that full cell using coated Li as anode shows superior stability for 500 cycles. From the cycling performance demonstrated in Figure 5c, it can also be seen that the coulombic efficiency of LFP/LATP/Li cell fluctuates with cycling whereas the cell with coated Li shows much more consistent coulombic efficiency. From the gradually increasing impedance in Figure S10 in the Supporting Information, it is speculated that the capacity fading for the cell using coated Li could be due to the depletion of liquid electrolyte as well as gradual degradation of the protective layer during prolonged cycling, which further leads to voltage polarization as shown in Figure 5c. The improved cycling performance in full cells further confirms the stabilizing effect of the coating layer on the interface between Li and SSEs.

In this study, a novel coating strategy for Li anode is proposed to quickly form an artificial nanocomposite protecting layer which consists of LiF, MgF_2, and B_2O_3, and serves as an artificial SEI that remains stable after repeated cycling in

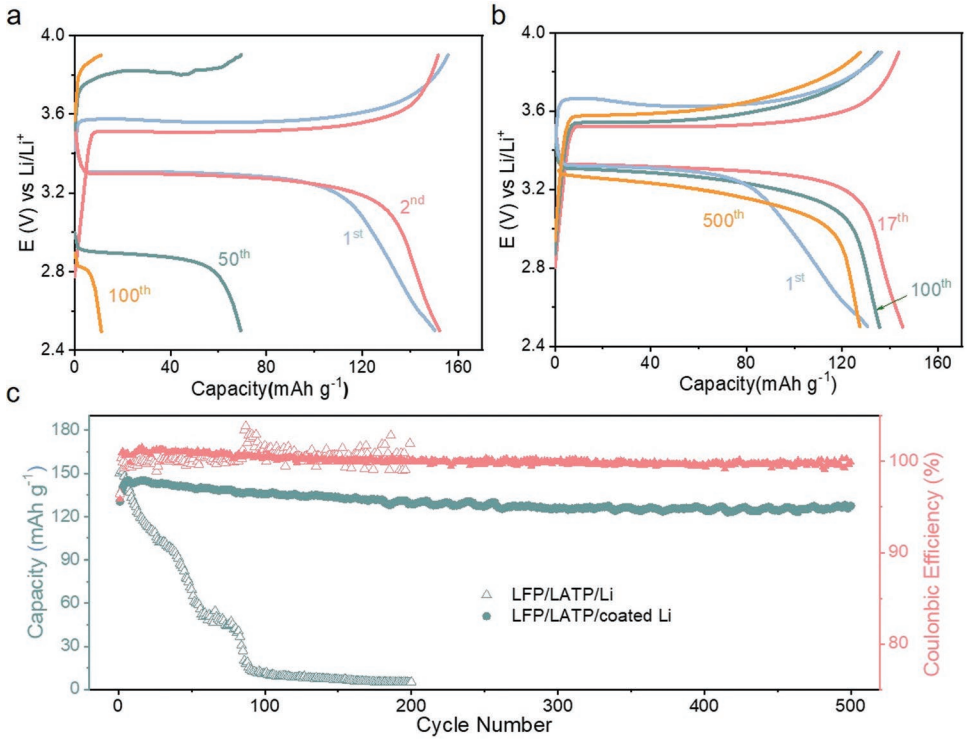

Figure 5. Voltage profiles of a) LFP/LATP/Li and b) LFP/LATP/coated Li cells at different cycles at the C-rate of 1.5 C. c) Cycling performances and coulombic efficiencies of LFP/LATP/Li and LFP/LATP/coated Li cells.

liquid electrolyte. By combining the coated Li with solid-state electrolyte, this layer inhibits the interfacial reaction between Li and LATP (i.e., reduction of Ti^{4+}) by blocking the physical contact. Due to the stable Li-LATP interface, the Li/LATP/Li symmetric cell exhibits excellent cycling stability for over 300 h of continuous Li plating/stripping. Moreover, the LFP/LATP/Li full cell also shows high capacity retention after 500 cycles. Overall, this work demonstrates a fast and universal method to stabilize the SEI layer for Li metal anode for both solid-state and liquid cells.

Experimental Section

Preparation of Coated Li: $LiBF_4$ (98%, Acros) and $Mg(ClO_4)_2$ (anhydrous, Aladdin) are dissolved in 1,2-dimethoxyethane (DME, 99.5%, Aladdin) with concentrations of 0.8 and 0.2 mol L^{-1}, respectively. 100 µL of the solution was then casted on Li metal foil with thickness of 0.6 mm to react for 30 s. The reacted Li foil was then washed by DME and dried under vacuum for 12 h before use.

Preparation of LATP Pellet: The solid electrolyte LATP was synthesized via a conventional solid-state reaction method. The starting materials $LiOH.H_2O$ (98%, Aladdin), Al_2O_3 (AR, Aladdin), $NH_4H_2PO_4$ (99%, Aladdin), and TiO_2 (99.99%, Aladdin) were mixed by ball milling using a ZrO_2 jar and balls for 10 h at a speed rate of 350 rpm. After mixing, the mixture was sintered at 850 °C for 6 h. The ball milling was repeated after sintering process. And the obtained powder with a weight of 0.4 g was pressed into pellet using a 12.2 mm diameter die and sintered at 950 °C for 6 h. The resulting pellets were polished to about 1 mm thick with sand paper.

LFP Electrode Preparation: LFP cathode material is mixed with carbon black and PVdF in *N*-methyl pyrrolidone at a mass ratio of 7:2:1 which was then coated on an Al foil, followed by drying at 80 °C. Then the LFP cathode was cut into pellets with a diameter of 10 mm. The pellets were further dried at 80 °C under vacuum overnight. The areal loading of active material is ≈1 mg cm^{-2}.

Characterization and Electrochemical Measurement: The structural characterization was performed by a Bruker D8 Advance powder XRD with 2θ in the range of 10°–70° with a step size of 0.05°. Morphology study and element distribution were performed using a scanning electron microscopy with energy dispersive spectrometer (SEM, Zeiss SUPRA-55), XPS (ESCALab220I-XL) was conducted to measure the chemical properties. Symmetric cells assembled by stacking LATP between two Li foils in a Swagelok cell. EIS were collected by an electrochemical workstation (1400 cell test system, Solartron) in the frequency range from 1 MHz to 0.1 Hz with 5 mV amplitude at room temperature. The lithium plating/stripping test was carried out by galvanostatic cycling with an automatic galvanostatic charge–discharge unit (Maccor, MC-16 Battery Test System) at room temperature. The cells were assembled in a glove box in Ar atmosphere. For better interfacial contact, a minimum amount (5 µL) of liquid electrolyte (1 mol LiFSI in DME) was added on each side of LATP pellet. To make sure the added liquid electrolyte was strictly separated by the solid electrolyte, the LATP pellet was surrounded by a polyimide film, where a hole with the size of LATP pellet is cut (shown in Figure S11 in the Supporting Information). The pressure between electrode and LATP pallet is ≈800 kg cm^{-2}. The performance of cells was also carried out by galvanostatic cycling with an automatic galvanostatic charge–discharge unit (Maccor, MC-16 Battery Test System) at room temperature. The LFP full cells were characterized by galvanostatic cycling at 1.5 C with a voltage range between 2.5 and 3.9 V versus Li/Li^+.

Supporting Information

Supporting Information is available from the Wiley Online Library or from the author.

Acknowledgements

L.Y. and Y.S. contributed equally to this work. This work was financially supported by grants from National Key R&D Program of China (2016YFB0700600), the National Natural Science Foundation of China (Nos. 51672012 and 51802224), Soft Science Research Project of Guangdong Province (No. 2017B030301013), and Shenzhen Science and Technology Research Grant (ZDSYS201707281026184).

Conflict of Interest

The authors declare no conflict of interest.

Keywords

lithium metal anodes, solid-electrolyte interfaces, solid-state electrolytes, surface coating

Received: November 4, 2019
Revised: December 17, 2019
Published online: January 20, 2020

[1] J. Lu, Z. Chen, F. Pan, L. A. Curtiss, K. Amine, *Nat. Nanotechnol.* **2016**, *11*, 1031.
[2] J. Lu, Z. Chen, F. Pan, Y. Cui, K. Amine, *Electrochem. Energy Rev.* **2018**, *1*, 35.
[3] J. Xiang, L. Yang, L. Yuan, K. Yuan, Y. Zhang, Y. Huang, J. Lin, F. Pan, Y. Huang, *Joule* **2019**, *3*, 2334.
[4] X. B. Cheng, R. Zhang, C. Z. Zhao, Q. Zhang, *Chem. Rev.* **2017**, *117*, 10403.
[5] D. Lin, Y. Liu, Y. Cui, *Nat. Nanotechnol.* **2017**, *12*, 194.
[6] J. B. Goodenough, *Nat. Electron.* **2018**, *1*, 204.
[7] B. Zhang, R. Tan, L. Yang, J. Zheng, K. Zhang, S. Mo, Z. Lin, F. Pan, *Energy Storage Mater.* **2018**, *10*, 139.
[8] C. Yang, K. Fu, Y. Zhang, E. Hitz, L. Hu, *Adv. Mater.* **2017**, *29*, 1701169.
[9] S. Xin, Y. You, S. Wang, H. C. Gao, Y. X. Yin, Y. G. Guo, *ACS Energy Lett.* **2017**, *2*, 1385.
[10] J. Janek, W. G. Zeier, *Nat. Energy* **2016**, *1*, 1.
[11] M. Monchak, T. Hupfer, A. Senyshyn, H. Boysen, D. Chernyshov, T. Hansen, K. G. Schell, E. C. Bucharsky, M. J. Hoffmann, H. Ehrenberg, *Inorg. Chem.* **2016**, *55*, 2941.
[12] H. Aono, E. Sugimoto, Y. Sadaoka, N. Imanaka, G. Adachi, *J. Electrochem. Soc.* **1990**, *137*, 1023.
[13] H. Kitaura, H. Zhou, *Adv. Energy Mater.* **2012**, *2*, 889.
[14] X. B. Zhu, T. S. Zhao, Z. H. Wei, P. Tan, G. Zhao, *Energy Environ. Sci.* **2015**, *8*, 2782.
[15] G. Yan, S. Yu, W. Yang, X. Li, H. Tempel, H. Kungl, R.-A. Eichel, M. Krüger, J. Malzbender, *J. Power Sources* **2019**, *437*, 226940.
[16] W. Lee, C. K. Lyon, J. H. Seo, R. Lopez-Hallman, Y. Leng, C. Y. Wang, M. A. Hickner, C. A. Randall, E. D. Gomez, *Adv. Funct. Mater.* **2019**, *29*, 1.
[17] W. Xu, J. Wang, F. Ding, X. Chen, E. Nasybulin, Y. Zhang, J.-G. Zhang, *Energy Environ. Sci.* **2014**, *7*, 513.
[18] J. A. Lewis, F. Javier, Q. Cortes, M. G. Boebinger, J. Tippens, T. S. Marchese, N. Kondekar, X. Liu, M. Chi, M. T. Mcdowell, *ACS Energy Lett.* **2019**, *4*, 591.
[19] J. Tippens, J. C. Miers, A. Afshar, J. A. Lewis, F. J. Q. Cortes, H. Qiao, T. S. Marchese, C. V. Di Leo, C. Saldana, M. T. McDowell, *ACS Energy Lett.* **2019**, *4*, 1475.
[20] H. Chung, B. Kang, *Chem. Mater.* **2017**, *29*, 8611.
[21] Y. Liu, C. Li, B. Li, H. Song, Z. Cheng, M. Chen, P. He, H. Zhou, *Adv. Energy Mater.* **2018**, *8*, 1702374.
[22] W. Zhou, S. Wang, Y. Li, S. Xin, A. Manthiram, J. B. Goodenough, *J. Am. Chem. Soc.* **2016**, *138*, 9385.
[23] Y. Liu, Q. Sun, Y. Zhao, B. Wang, P. Kaghazchi, K. R. Adair, R. Li, C. Zhang, J. Liu, L. Kuo, Y. Hu, T. Sham, L. Zhang, R. Yang, S. Lu, X. Song, X. Sun, *ACS Appl. Mater. Interfaces* **2018**, *10*, 31240.
[24] Q. Cheng, A. Li, N. Li, S. Li, A. Zangiabadi, T. De Li, W. Huang, A. C. Li, T. Jin, Q. Song, W. Xu, N. Ni, H. Zhai, M. Dontigny, K. Zaghib, X. Chuan, D. Su, K. Yan, Y. Yang, *Joule* **2019**, *3*, 1510.
[25] Y.-C. Jung, M.-S. Park, C.-H. Doh, D.-W. Kim, *Electrochim. Acta* **2016**, *218*, 271.
[26] Q. Zhang, F. Ding, W. Sun, L. Sang, *RSC Adv.* **2015**, *5*, 65395.
[27] L. Yang, Z. Wang, Y. Feng, R. Tan, Y. Zuo, R. Gao, Y. Zhao, L. Han, Z. Wang, F. Pan, *Adv. Energy Mater.* **2017**, *7*, 1701437.
[28] D. Li, L. Chen, T. Wang, L. Z. Fan, *ACS Appl. Mater. Interfaces* **2018**, *10*, 7069.
[29] Q. Ma, X. X. Zeng, J. Yue, Y. X. Yin, T. T. Zuo, J. Y. Liang, Q. Deng, X. W. Wu, Y. G. Guo, *Adv. Energy Mater.* **2019**, *9*, 1.
[30] H. Zhai, P. Xu, M. Ning, Q. Cheng, J. Mandal, Y. Yang, *Nano Lett.* **2017**, *17*, 3182.
[31] R. DeWees, H. Wang, *ChemSusChem* **2019**, *12*, 3713.

